


Dependence of Photoluminescence Emission on Excitation Power and Temperature in Highly Doped 6H-SiC

Abebe T. Tarekegne^{1,*}, Xiaodong Shi,¹ Yulin Gan², Yunzhong Chen² and Haiyan Ou^{1,†}

¹*Department of Photonics Engineering, Technical University of Denmark, DK-2800, Kgs. Lyngby, Denmark*

²*Department of Energy Conversion and Storage, Technical University of Denmark, DK-2800, Kgs. Lyngby, Denmark*

 (Received 20 December 2019; revised manuscript received 6 January 2020; accepted 13 April 2020; published 1 June 2020)

The excitation power and temperature dependences of photoluminescence (PL) emission in 6H polytype of silicon carbide are investigated extensively. A sublinear power-function dependence of the donor-acceptor pair emission intensity on the excitation power is explained by a rate-equation model. A very low power exponent ($k = 0.3$) in a power-law dependence of PL intensity on the excitation power of B-N codoped 6H-SiC at room temperature indicates that three-particle Auger recombination is the main carrier recombination pathway. Auger recombination in an Al-N codoped SiC does not manifest as strongly as that of the B-N codoped sample due to high density of ionized impurities which capture the nonequilibrium carriers faster. The ionized impurities form localized potential wells due to their random distribution, which is revealed by a blue shift of the PL band with increasing excitation intensity (approximately 16 meV per decade) and with decreasing temperature. Low-temperature Hall-effect measurement of the Al-N codoped sample confirms the high density of ionized impurities and significantly reduced ionization energy of dopant states by approximately 53 meV due to the high dopant densities. These results could lead to realization of tunable SiC-based light sources in severe operating conditions.

DOI: [10.1103/PhysRevApplied.13.064002](https://doi.org/10.1103/PhysRevApplied.13.064002)

I. INTRODUCTION

Silicon carbide (SiC) has unique properties such as large bandgap, high thermal conductivity, chemical inertness, large breakdown voltage, possibility of n -type and p -type doping, and radiation resistance, which makes it a leading semiconductor for high-power electronics [1]. Recently, it has attracted considerable research attention for photonics applications, such as white light sources [2–4], a host of quantum emitters [5,6], and as a material platform for nonlinear optics [7–9]. The possibility of achieving broadband light emission, single photon emission, and integrated photonic circuits [10–13], in addition to its mature nanoprocessing technology, makes it a promising platform for an all-SiC-based integrated optoelectronic chip. The possibility of rare-earth metal-free wavelength conversion with SiC is suitable for sustainability and in biomedical applications where biocompatibility is relevant.

In the lighting industry, SiC is used as a substrate to grow GaN-based high-power LEDs due to its high thermal conductivity (approximately 10 times that of sapphire

[14,15] and small lattice mismatch with GaN (3.5%) [16]. With suitable acceptor and donor doping, SiC emits broadband visible light in the donor-acceptor pair (DAP) recombination process [17]. Al-N codoped 6H-SiC emits broadband blue light and B-N codoped SiC emits broadband yellow light, which can be combined to produce a white light. The yellow emission from B-N codoped SiC, where a PL quantum yield of up to 30% is achieved at room temperature (RT) [18], has a better red spectral coverage than even the popular yellow phosphor (yttrium aluminum garnet doped with Ce^{3+}). The performance degradation and quenching at high photon flux of the well-known phosphors lead to gradual decline in the efficiency and color quality [19], driving the search for alternative light converters for laser lighting where laser flux is expected. Owing to its broadband emission and excellent thermal attributes, SiC-based wavelength converters can be ideal for laser lighting applications where high thermal load is expected [20]. For practical applications of fluorescent SiC in the high-power wavelength conversion, improving the conversion efficiency and investigation of high excitation power property are crucial.

An important consideration for high-power lighting applications of fluorescent SiC is the excitation power dependence of the PL intensity. In many other semiconductors, the PL intensity follows a power-law dependence

*atil@fotonik.dtu.dk

†haou@fotonik.dtu.dk

on excitation power [21–25]. Mathematically,

$$I_{\text{PL}} \propto L_{\text{ex}}^k, \quad (1)$$

where I_{PL} is the PL intensity, L_{ex} is the excitation power, and k is the power exponent, where $1 < k < 2$ for excitonlike transitions and $k < 1$ for free-to-bound and DAP transitions [26]. The value of the power exponent indicates the trend in wavelength conversion efficiency with increasing excitation power. A value of k as close as possible to one implies that the conversion efficiency at high excitation powers maintains that of the low excitation powers. In other words, the conversion efficiency does not decline with increasing excitation power. The optimization of the power exponent in SiC requires detailed physical understanding of the radiative recombination mechanisms.

Excitation power dependent PL measurements can also reveal physical insight into the perturbation of bands. A shift of the PL band with increasing excitation power is observed in highly doped and compensated semiconductors and is attributed to the high density of ionized impurities [27]. Gislason *et al.* reported that semi-insulating Li-doped GaAs shows an excitation power-dependent PL peak position that shifts to lower energies with increasing compensation [28]. Similarly, Guo *et al.* and Baume *et al.* reported that DAP emissions in ZnO and nitrogen-doped ZnSe, respectively, show a logarithmic increase in peak energy with the excitation power [29,30]. In highly doped and compensated crystals, the statistically random distribution of charged impurities creates an irregular fluctuation of potential which perturbs the band states of the semiconductor crystal [31]. This, in turn, creates localized potential wells that affect the emission spectrum and carrier-transport property. High concentrations of donors and acceptors in excess of 10^{18} cm^{-3} are required in SiC for efficient wavelength conversion [32]. In this case, high density of ionized impurities perturbs the band structure [28], which affects the emission property as well as the carrier transport property [33–35].

In this article, the excitation power and temperature dependences of the PL intensity of highly doped 6H-SiC are systematically investigated. The investigations reveal that PL intensity follows a power-law dependence on the excitation power, where the power exponent reveals the physical carrier recombination mechanisms. Furthermore, for highly doped and compensated 6H-SiC, we observe a shifting PL band with the change of excitation power and temperature that shows the formation of localized potential wells.

II. EXPERIMENTS

Two kinds of 6H-SiC epilayers, namely boron and nitrogen (B-N) codoped and aluminum and nitrogen (Al-N) codoped samples that emit broadband yellow and blue,

respectively, are used for the investigations. The samples are grown by fast sublimation growth process (FSGP) [36] on 1.4° off-oriented and 1° off-oriented *n*-type SiC (1000) substrate for B-N and Al-N codoped samples, respectively. The desired doping densities are achieved by introducing the dopants during the source material growth, which is subsequently used for the sublimation epitaxy. The growth temperature in the FSGP process is 1920°C for the Al-N codoped 6H-SiC and 1950°C for the B-N codoped 6H-SiC. The N concentration of the Al-N codoped epilayer is enhanced by performing the growth in 3 mbar N_2 ambient. The concentrations of Al and N in the Al-N doped sample near the surface are 1.8×10^{18} and $1.1 \times 10^{19} \text{ cm}^{-3}$, respectively, whereas the concentrations of B and N in the B-N doped sample are 1.1×10^{18} and $2.9 \times 10^{18} \text{ cm}^{-3}$, respectively, as measured by time-of-flight secondary ion mass spectrometry (TOF SIMS). The thicknesses of the Al-N epilayer and substrate are 216 and $256 \mu\text{m}$, respectively, as measured by a standard micrometer caliper. Similarly, the epilayer and substrate thicknesses of the B-N sample are 150 and $250 \mu\text{m}$, respectively.

For the PL measurements, the samples are placed in a vacuum chamber, which allows the variation of the sample temperature using an Oxford cryogenic system. The sample temperature is varied to probe different emission mechanisms that dominate the emission process at different temperatures. For the investigations of the excitation power dependence of the PL emission property, two continuous-wave lasers from Oxixus emitting at 375 nm are used. For the high injection level measurements, the laser beam is focused directly on the sample, by focusing lenses, down to a beam spot size of $112 \mu\text{m}$. The laser used in these measurements has a maximum power of 400 mW. At the highest incident excitation power density of 750 W cm^{-2} , no sign of damage or PL degradation is observed, which establishes the prospect of fluorescent SiC for high-power lighting. For the low injection measurements, a laser with a maximum output of 50 mW is employed. In these measurements, the near ultraviolet (NUV) excitation is focused on the sample through a microscope objective. The power level of the lasers is varied using a laser control system where the lasers are operated in a constant laser output mode so that the output power is stabilized. The PL signal is collected by a microscope objective and is coupled to an Andor spectrometer (SR-3031-A spectrograph with DU-420-0E CCD).

The temperature-dependent free-carrier density is measured by a Hall-effect measurement system in a van der Pauw configuration. A cryogenic measurement system is employed to characterize the magnetotransport with temperature from 2 K to room temperature and a perpendicular magnetic field of up to 2 T. The Ohmic contacts are fabricated by depositing 200 nm thick Ni using an electron beam evaporator and subsequent rapid thermal annealing at 1050°C in a vacuum for 5 min.

III. RESULTS AND DISCUSSION

A. Excitation power dependence of the PL intensity

Figure 1(a) shows the measured PL emission spectra from the Al-N codoped 6H-SiC sample at several incident excitation power levels at 77 K. Figures 1(b) and 1(c) shows a log-log plot of the power dependence of the PL peak intensity of the Al-N doped sample at different temperatures. The log-log plot can be fitted well with a linear curve over an incident power range of approximately three orders of magnitude. This means that the PL intensity and the excitation power can be related by a power-law

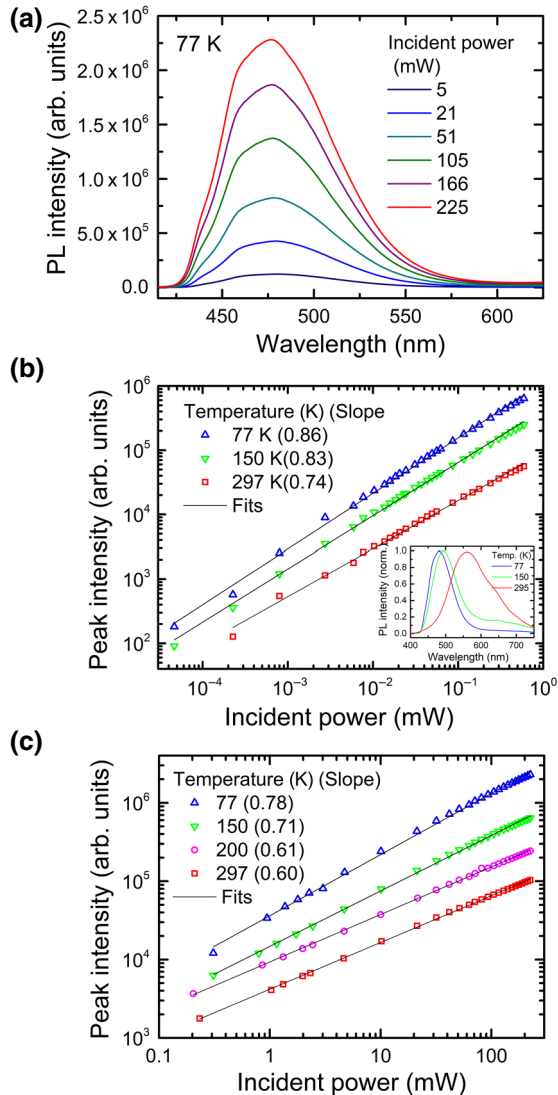


FIG. 1. PL emission properties of Al-N codoped 6H-SiC. (a) Emission spectra at 77 K and at different excitation power levels. (b) Log-log plot of the PL peak intensity versus the incident excitation power at low-excitation power range and (c) at high-excitation power range at several temperatures. The black solid curves are linear fits of $\log(I_{PL})$ vs $\log(L_{ex})$. The inset in (b) shows the normalized spectra of the PL emission with incident power of 0.6 mW at different temperatures.

function. The slope in the linear fit of $\log(I_{PL})$ vs $\log(L_{ex})$ is the power exponent k . The measurements show that the power exponent for the Al-N doped sample is in the range of $0.6 < k < 1$ for all temperatures, which is expected for a DAP recombination [26]. Comparison of Figs. 1(b) and 1(c) shows that the power exponents are higher at low injection powers than at high injection powers at a given temperature.

The inset in Fig. 1(b) shows the emission spectra at an incident power of 0.66 mW and temperatures of 77, 150 and 295 K. The different power exponents at different temperatures are partially attributed to differences in the radiative recombination pathways, which are attested by the spectral modifications. At low temperatures, the dominant emission mechanisms are Al-N DAP transition [37] and recombination of a weakly bound electron and a tightly bound hole at an intrinsic defect known as the D_1 center [38]. At high temperatures, these two emission mechanisms weaken significantly and the B-N DAP contribution dominates the radiative recombination process. The boron-related emission appears due to the diffusion of boron from the substrate to the epilayer during the growth. The evolution of the emission mechanisms is attributed to differences between the temperature dependences of carrier capture rates for the different emission mechanisms [39]. A PL emission of the Al-N sample quenches as temperature increases due to thermally activated hole capture by a nonradiative trap.

The excitation power-dependent measurement results for the B-N codoped sample are shown in Fig. 2. Similar to the Al-N codoped 6H-SiC, the PL intensities in B-N codoped 6H-SiC show a power-function relationship with the excitation power. At room temperature and a high excitation power range, the PL intensity dependence can be described by, $I_{PL} \propto L_{ex}^{0.3}$. At 100 K, the power exponent increases such that $I_{PL} \propto L_{ex}^{0.67}$. The power exponent is higher at low excitation powers than at high excitation powers. Furthermore, at very low incident powers, the PL intensity increases linearly with the excitation power, i.e., $k \approx 1$.

The inset in Fig. 2(b) shows the normalized emission spectra at different temperatures with an incident power of 225 mW. Boron doping introduces two acceptor complexes (D and D^* center) with two different acceptor energy levels [40]. As a result, two B-related DAP emission mechanisms are involved. At low temperatures, DAP recombination through the deeper (D^*) acceptor is more prominent than the shallower D center and vice versa at high temperatures. At 300 K, the spectrum with a peak of approximately 580 nm is mainly due to the DAP emission involving the D center. At 100 K, the dominant radiative emission mechanism involves the D^* center and its peak emission wavelength is located approximately at 650 nm. To analyze the two emission mechanisms separately, PL intensities away from their peaks are selected to reduce the

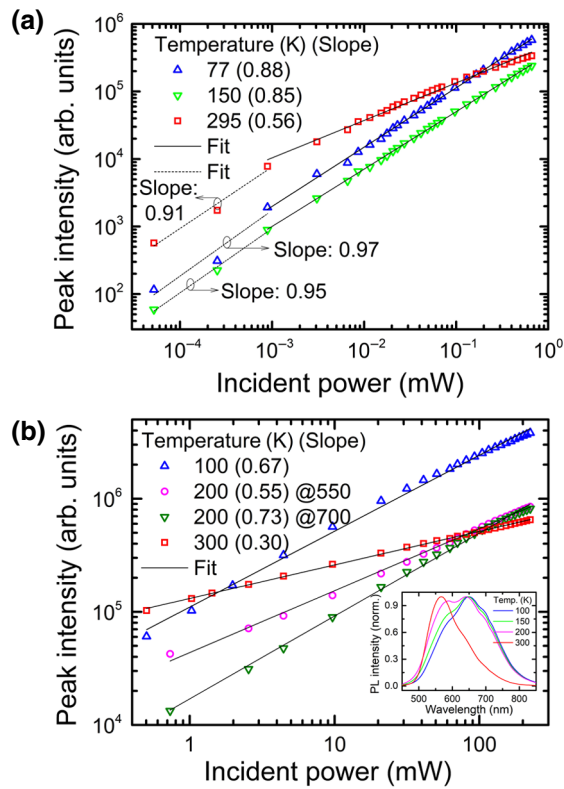


FIG. 2. The PL peak intensity vs excitation power of the B-N codoped 6H-SiC at several temperatures: (a) at low-excitation power range, (b) at high-excitation power range. The inset in (b) shows the normalized spectra of the PL emission at different temperatures. The black solid and dotted lines are linear fits of $\log(I_{PL})$ vs $\log(L_{ex})$.

contributions from the other emission pathway, since the emission spectra overlap slightly. Figure 2(b) shows the PL intensities at 200 K as a function of excitation power at 550 nm (mainly D contribution) and 700 nm (mainly D* contribution). At 200 K, the two emission mechanisms have comparable contributions. The power dependencies of the two radiation centers are different with power exponents of 0.55 and 0.73 for PL intensities at 550 and 700 nm, respectively. The differences in slopes can be attributed to the differences in the densities and carrier capture rates of the acceptor complexes.

B. Modeling the carrier recombination process in SiC

The carrier recombination dynamics in 6H-SiC is complicated because of the several radiative and nonradiative transitions. A single type of radiative transition has further dependencies on the location of dopants on inequivalent lattice sites. For example, the donor energy levels depend on the type of lattice site, which, in turn, affects its carrier capture and emission properties [41]. For semiquantitative interpretation of the excitation power dependences of the PL emissions in 6H-SiC, a simplified rate-equation

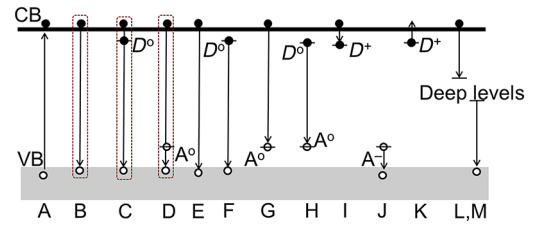


FIG. 3. Radiative and nonradiative transitions in a donor and acceptor codoped SiC. The black circles represent electrons and the open circles represent holes. (A) Optical excitation by above bandgap photons, (B) free exciton recombination, (C, D) bound exciton recombination, (E) Auger recombination (three-particle process), (F) radiative recombination of free hole and neutral donor, (G) radiative recombination of free electron and neutral acceptor, (H) donor-acceptor recombination, (I, J) nonradiative transition of free electron and hole to ionized donor and acceptor respectively, (K) excitation of electron from neutral donor and (L, M) nonradiative capture of free electron and hole by deep levels. The arrow indicates the direction of electron transfer.

model proposed by Schmidt *et al.* [26] is applied. The simplified free-carrier transition pathways are shown in Fig. 3. We assume that the electron-hole pairs are generated by above bandgap photon excitation (process A) and they can recombine by the following transitions: free exciton recombination (B), donor and acceptor bound exciton recombination (C and D, respectively), three-particle Auger recombination (E), neutral donor and free hole recombination (F), free-electron and neutral-acceptor recombination (G), DAP recombination (H), nonradiative capture of free electrons and holes to ionized donors and acceptors (I and J, respectively) and nonradiative capture of electrons and holes by deep defect levels (L, M). In addition, the thermal excitation of electrons from the donor states (K) can occur.

6H-SiC has a rather large exciton binding energy of 78 meV [42], which can survive dissociation at room temperature. However, exciton recombination is prominent in a crystal with fewer defects and high purity levels. The exciton peaks are observed in lightly doped SiC samples where the doping level is below 10^{17} cm^{-3} [43]. In our samples, where the doping concentration is high ($>10^{18} \text{ cm}^{-3}$), the exciton recombination is unlikely, and we do not observe exciton-related emission peaks from the samples in the temperature range of our measurements (77–300 K). Thus, we assume that recombination through the excitons is negligible. Moreover, the known acceptor states with the dopants in our samples are rather deep with ionization energy higher than 200 meV [37,44]. In this case, we assume that the thermal induced transfer of holes from the acceptor states to the valence band is negligible.

The PL emission energies in the samples are significantly shifted from the bandgap energy. For example, the emission peak of the Al-N sample is shifted by approximately 0.5 eV from the bandgap energy [See

Fig. 1(a)]. Therefore, the emissions involve deep acceptors and are either a DAP or a free-electron-to-acceptor (FA) recombination. Furthermore, the typical energy levels of nitrogen donors are relatively deep, with binding energies of about 85 meV at hexagonal and 140 meV at cubic sites at lower doping levels [45]. It can be expected that a significant majority of captured electrons will stay on the donor state in the temperature range of the measurement. In addition, carriers bound on the dopant states will have a higher probability of radiative recombination as free carriers can be quickly captured by the nonradiative trap centers. From these considerations, one can conclude that DAP is the main radiative recombination mechanism in our samples.

The emission intensities of DAP and FA depend on the densities of free electrons, neutral acceptors, and donors. The dynamic relationship between the relevant densities can be described by the following set of coupled differential equations as proposed by Schmidt *et al.* [26]:

$$\frac{dn}{dt} = aL_{\text{ex}} - en^3 - gnN_A^0 - in(N_D - N_D^0) - nN_{\text{deep}}^0, \quad (2)$$

$$\frac{dN_D^0}{dt} = in(N_D - N_D^0) - fpN_D^0 - hN_A^0N_D^0, \quad (3)$$

$$\frac{dN_A^0}{dt} = jp(N_A - N_A^0) - gnN_A^0 - hN_A^0N_D^0. \quad (4)$$

In Eqs. (2)–(4), n and p are the densities of the free electrons and holes, respectively; N_A^0 , N_D^0 , and N_{deep}^0 are the concentrations of neutral acceptors, neutral donors, and deep defects, respectively; N_D and N_A are the concentrations of donors and acceptors, respectively. The coefficients a , e , f , g , h , i , j , l are the transition rates of the processes A , E , F , G , H , I , J , L respectively.

The measurements show that the PL intensities of the samples follow the power-law dependence on the excitation power, i.e., $I_{\text{PL}} \propto L_{\text{ex}}^k$. The PL intensity from DAP recombination is proportional to the product of neutral-acceptor and donor densities ($N_A^0 N_D^0$). In a steady-state condition and with the assumption of equal density of free holes and electrons, the comparison of Eqs. (3) and (4) shows that the neutral-acceptor and donor concentration has similar dependence on excitation laser power, i.e., $N_D^0(L_{\text{ex}}) \propto N_A^0(L_{\text{ex}})$. From these relationships, it can be expected that the density of ionized donors and acceptors has a power-law dependence on the laser excitation power with power exponent of $\frac{k}{2}$. Similarly, the concentration of neutral donors can be defined by solving from Eq. (3) as,

$$N_D^0 = -\frac{n(f+i)}{2h'} + \frac{1}{2h'} \sqrt{4h'inN_D + n^2(i+f)^2}. \quad (5)$$

Here, $N_A^0(L_{\text{ex}\delta}) = \gamma N_D^0(L_{\text{ex}})$ is assumed, and $h' = \gamma h$, where γ is a constant. For simplicity, we consider two limiting cases to correlate the free-electron and neutral-donor densities. If $N_D \gg n(i+f)^2/(4h'i)$, then it can be

deduced from Eq. (5) that $N_D^0 \propto \sqrt{n}$. Similarly if $N_D \ll n(i+f)^2/(4h'i)$, then the neutral-donor density can have a linear relationship with free-electron density, i.e., $N_D^0 \propto n$.

To correlate the emission PL intensity with excitation power, the free-carrier and neutral-dopant densities need to be defined by solving the differential equations. Direct solution of Eqs. (2)–(4) is not straightforward due to the lack of complete data on SiC carrier-transition dynamics and complexity involving several recombination pathways and site-dependent properties. However, important conclusions can be drawn from the interpretation of the measurements by considering the limiting cases. In the case of very high injection levels, the three-particle Auger recombination process will be the main recombination mechanism. In this case, Auger recombination rate involving two electrons and a hole can be expressed as, $R_{\text{Auger}} = \gamma_A^{eeh} n^2 p \propto n^3$, where γ_A^{eeh} is the Auger recombination coefficient. Applying Eq. (2) in a steady-state condition, free-carrier density can be related to the excitation laser power as, $n \propto \sqrt[3]{L_{\text{ex}}}$. At the low and intermediate injection levels, where Auger recombination is not the limiting factor, the relationship between the free-carrier density and laser power can be approximated from Eq. (2) as, $n \propto L_{\text{ex}}^\beta$ where β can vary between 0.5 and 1 depending on the dominant recombination mechanism.

The PL intensities for DAP and FA recombination can be defined, respectively, as

$$I_{\text{DAP}} \propto N_D^0 N_A^0, \quad (6)$$

$$I_{\text{FA}} \propto n N_A^0. \quad (7)$$

Using Eqs. (6) and (7) as well as the aforementioned limiting cases, the PL intensities can be related to the excitation power. Based on the relative comparison between dopant density and free-carrier density (N_D and n) as well as the contribution of Auger recombination in the carrier relaxation, four limiting scenarios can arise. For $N_D \gg n(i+f)^2/(4h'i)$ and a dominant Auger recombination, $I_{\text{DAP}} \propto L_{\text{ex}}^{0.33}$ and $I_{\text{FA}} \propto L_{\text{ex}}^{0.5}$. In the low injection conditions where $N_D \gg n(i+f)^2/(4h'i)$ and no significant Auger recombination contribution, $I_{\text{DAP}} \propto L_{\text{ex}}^k$, where $0.67 < k < 1$. If the free-to-acceptor recombination rate is negligible and the portion of ionized donors is low, then $k \approx 1$.

Similarly for $N_D \ll n(i+f)^2/(4h'i)$ and a dominating Auger recombination, $I_{\text{DAP}} \propto L_{\text{ex}}^{0.67}$. Finally, if $N_D \ll n(i+f)^2/(4h'i)$ and Auger recombination contribution is insignificant, $I_{\text{DAP}} \propto L_{\text{ex}}^k$, where $1 < k < 2$, which is the only case that results in a superlinear power dependence. This scenario is unlikely in our samples where the dopant concentrations are very high. As a result, the excitation power dependence of DAP emission intensity is a sublinear power function in SiC and other semiconductors.

With these limiting cases, the overall characteristics of the measured excitation power dependences of the PL

intensity can be explained. The observed trend in measurements that the power exponent is higher at the low excitation power ranges than at the high excitation power ranges indicates the higher contribution of Auger recombination in the latter. At RT, the PL power dependence on excitation power for the B-N doped sample has a power exponent of 0.3, which is close to 0.33 and is expected for a dominant Auger recombination pathway involving three photogenerated carriers. A similar incident power for the B-N doped sample at low temperatures and Al-N doped sample does not show such a low power exponent. We note here that the Al-N DAP emission is quenched as temperature increases and its contribution at RT is very weak. The power exponents in the Al-N doped sample vary within $0.6 < k < 1$. The values imply reduced contribution from Auger recombination or Auger recombination limited by free-electrons from the dopants, i.e., when photogenerated free-carrier density is much smaller than the free-electron contributions from the donors. In such cases, the Auger recombination can be limited by the dopant concentrations, where $R_{\text{Auger}} = \gamma_A^{eh} N_D^2 p \propto p$. Here, $p \propto L_{\text{ex}}$ and a power exponent of $0.67 < k < 1$ can be obtained.

The analysis of the PL emission spectra, which is discussed in the subsequent sections, shows that the Al-N doped sample contains a higher density of ionized impurities than the B-N doped sample which can quickly capture nonequilibrium carriers in competition with the Auger recombination. At low temperatures, the emission intensity of the Al-N sample is more efficient than the B-N samples. The improved efficiency in the highly doped and compensated SiC sample could be due to the relatively reduced contribution from the nonradiative Auger recombination process. The exponent value of the Al-N doped sample could alternatively be interpreted as Auger recombination entangled with nonradiative traps such as the double intrinsic defects known as the E1/E2 centers [46], where the contribution of nonradiative traps increases the power exponent to higher values.

At very low excitation powers of the order 10^{-4} mW, the power dependence is close to 1 ($k \approx 1$) for the B-N doped sample. A power exponent value close to 1 indicates an insignificant contribution from the Auger recombination process. In this case, $N_D \gg n(i+f)^2/(4h'i)$ and the density of neutral donors (acceptors) will have a square root function of the free-carrier density. The free-carrier density increases almost linearly with excitation power according to the Shockley-Read-Hall process. The nearly linear relationship between the PL intensity and the excitation power is not observed for the Al-N sample due to the Auger contribution involving the free carriers from the donor states even at low excitation powers.

The different slopes (power exponents) at different temperatures can be attributed to the differences in the contributions of radiative recombination mechanisms and temperature-dependent changes of carrier capture rates.

As shown in Eq. (5), the densities of neutral donors and acceptors, thus PL intensity, depend on the carrier capture dynamics and the density of emission centers for each radiation mechanism. High capture rate by the donors can result in a faster trapping of the free carriers against the Auger recombination process. In both samples, the dominant emission mechanisms change between temperatures of 77 and 300 K, which will influence the power dependence property. One can also expect that increased density of free carriers due to thermal ionization at elevated temperatures facilitates Auger recombination process. In general, it is observed that the power exponent for a given emission process decreases with increasing temperature, which indicates an increased contribution of the Auger recombination process.

For efficient wavelength conversion in SiC at high excitation powers, the decline of the conversion efficiency as the excitation power increases needs to be mitigated. This requires the power exponent in the power-law dependence to approach one. Comparison of the Al-N and B-N 6H-SiC reveals that the power exponent can be improved by reducing the Auger recombination process, for example, by inclusion of a high density of donors and acceptors and a high level of compensation. In a compensated SiC crystal, ionized impurities capture the photoexcited carriers quickly, competing against the Auger recombination process.

This investigation clarifies the synergy between the radiative and nonradiative carrier recombination pathways. This is important for improving the wavelength conversion efficiency which will help the realization of SiC-based sources for future lighting applications, such as laser lighting, chip-level source for all-SiC-based integrated optoelectronic circuits, and biocompatible *in vivo* illumination.

C. Excitation power dependence of the PL spectrum

In addition to the PL intensity, the emission spectrum is analyzed carefully as the excitation power changes. We observe a peculiar shift in the emission spectra to higher energy as we increase the excitation power for the Al-N codoped sample. Figure 4(a) shows the dependence of the PL peak on the excitation power for the Al-N doped sample at 77 and 150 K. The inset shows representative emission spectra near the emission peak at 77 K, which depicts the PL peak (ω_p) shifting from 2.55 to 2.58 eV (a shift of ~ 6 nm) as the excitation power changes from 21 to 662 μW . This is a significant shift of approximately 16 meV per decade increase in the excitation power. More importantly, the emission peak energy increases logarithmically with the excitation power, such that $L_{\text{ex}} \propto \exp(\frac{\omega_p}{\gamma_s})$ where γ_s is a coefficient that represents the energy shift. This dependence is expected for semiconductors with a high density of ionized impurities, where the statistical distribution of the ionized impurities creates fluctuating

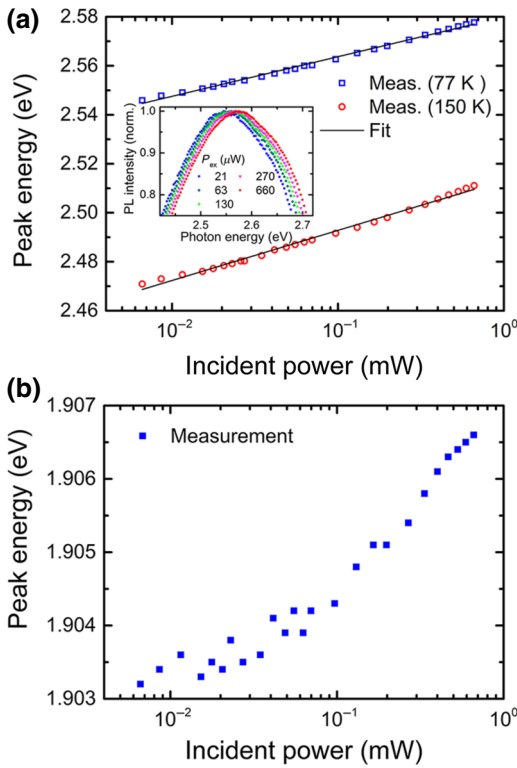


FIG. 4. (a) Emission peak energy vs incident excitation power of the Al-N codoped 6H-SiC at 77 and 150 K. The black curve is the linear fit of ω_p vs $\log(L_{ex})$ where the slopes are 16 meV/dBm and 21 meV/dBm for 77 and 150 K, respectively. The inset shows the PL curves near the emission peak at selected excitation powers. (b) Emission peak energy versus excitation power for the B-N codoped sample at 77 K.

potential. From the linear fits of the emission peak energy versus logarithm of the incident power, the value of γ_s is estimated to be 6.9 meV at 77 K and 9.1 meV at 150 K.

The emission peak shift for the B-N sample at 77 K is shown in Fig. 4(b). The peak shift with increasing excitation power is less than 4 meV, while the excitation power changes by two orders of magnitude. The dependence of the peak energy on the excitation power does not show a clear logarithmic dependence on the excitation power for the B-N doped sample as is in the fluctuation potential model. The lack of significant shift in the emission spectrum for the B-N sample is due to the lower density of ionized impurities.

The high density of randomly distributed ionized impurities results in the smearing of the energy states [27]. This phenomenon is shown schematically in Fig. 5. Shallow donors and acceptors lose their identity by mixing with the respective conduction and valance bands, forming band-tail states. The deep acceptor and donor states of those presented in the Al-N codoped SiC are strongly bound and their energy levels shift along with the perturbed band states. As a result, the DAP emission energy is reduced as shown in Fig. 5(b). The average depth of the potential well

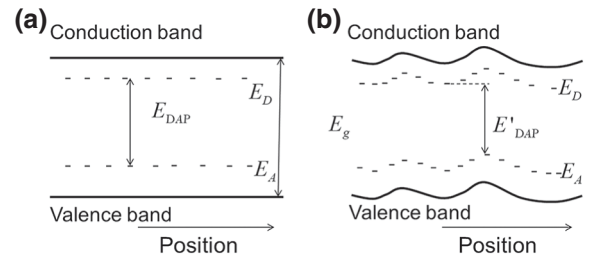


FIG. 5. Schematic representation of the perturbation of the band states due to charged impurities: (a) lightly doped crystal, (b) highly doped crystal with high density of charged impurity. E_g is the bandgap energy in a pure crystal, E_A is the acceptor energy level, and E_D is the donor energy level. E_{DAP} is emitted photon energy in a donor-to-acceptor transition. E'_{DAP} is the reduced emitted photon energy in a in perturbed band.

for n -type semiconductors depends on the free-electron density (n) and total density of charged impurities N_t ,

and is given by $\zeta(n, N_t) = \left(\frac{e^2}{4\pi\epsilon_0\epsilon} \right) \left(\frac{N_t}{n} \right)^{\frac{2}{3}}$ where e , ϵ_0 , ϵ

are the electronic charge, the dielectric permittivity, and the dielectric coefficient, respectively [31]. It can thus be expected that the potential-well depth increases with the concentration of the charged impurity but decreases with the free-charge density.

Considering the effect of the fluctuation potential, the photon energy $h\nu$ of the DAP emission is lowered by twice the average potential-well depth $\zeta(n, N_t)$, such that $h\nu = E_g - (\Delta E_D + \Delta E_A) + \frac{e^2}{4\pi\epsilon r} - 2\zeta$, where E_g , ΔE_D , ΔE_A , and $\frac{e^2}{4\pi\epsilon r}$ are the bandgap energy, the donor ionization energy, the acceptor ionization energy, and the Coulomb potential, respectively. As we increase the free-carrier density with the laser excitation, the average depth of the potential well decreases due to the screening of the fluctuating potential by the photogenerated electrons and holes. As a result, the PL emission shifts to higher energy, which is consistent with the measurements shown in Fig. 4(a). The lower value of the energy shift coefficient at 77 K than at 150 K is due to the smaller capture rate of deep wells at lower temperatures.

It can also be expected that increasing the excitation intensity favors the DAP recombination through close pairs such that the Coulomb potential increases and subsequently shifts the emission energy to higher energies. However, the contribution is expected to be less than the measured shift. This is supported by the measured shift in the B-N doped sample, where the shift is measured to be less than 2 meV per decade change of the excitation power. Therefore, the main PL band shifting mechanism is attributed to the perturbation of the band states due to the high density of charged dopants.

To examine the level of compensation in the Al-N doped sample directly, we perform the Hall-effect measurement that enables us to estimate the free-electron density, the

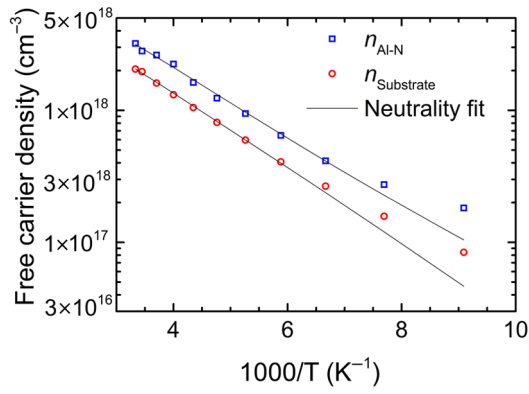


FIG. 6. Free-electron density of the epilayer and substrate ($n_{\text{Al-N}}$ and $n_{\text{substrate}}$ respectively) as a function of temperature for the Al-N doped sample measured by the Hall-effect system in a van der Pauw configuration. The black curves are the fits of the measurement data by the neutrality equation (Eq. 8).

density of compensating centers, and the donor ionization energy. The measured densities of free carriers of the epilayer and the substrate of the Al-N doped 6H-SiC are shown in Fig. 6. The measured data are fitted using the least-square method with the neutrality equation where the free-carrier density n is given by [47]

$$n + N_{\text{comp},A} = \frac{N_{D,h}}{1 + (g_D n / N_C) \exp(\Delta E_{D,h} / k_B T)} + \frac{N_{D,c}}{1 + (g_D n / N_C) \exp(\Delta E_{D,c} / k_B T)}, \quad (8)$$

where $N_{\text{comp},A}$ is the density of the compensating centers including acceptors, $N_{D,h}$ and $N_{D,c}$ are the density of donors at the hexagonal and cubic sites, $\Delta E_{D,h}$ and $\Delta E_{D,c}$ are the ionization energies of nitrogen donors at the hexagonal and cubic sites, g_D is the degeneracy factor for donors, and N_C is the effective density of state in the conduction band, which is given by $N_C = 2M_C(2\pi m_{de} k_B T / h^2)$. Here, M_C is the number of conduction band minima ($M_C = 6$) and m_{de} is the effective electron mass for the density of states in the conduction band ($m_{de} = 0.27m_0$), m_0 is electronic mass, h is the Planck constant, T is the temperature, and k_B is the Boltzmann constant. For the fitting, it is assumed that there are three kinds of inequivalent lattice sites (two cubic and one hexagonal) in equal proportions [45]. The two cubic sites have approximately the same ionization energy [48] and are treated as one site with twice the density of the hexagonal site. Furthermore, we assume that the dopant ionization energy decreases equally for the cubic and hexagonal sites at high doping levels.

As shown in Fig. 6, the measured free-electron densities are well fitted with the neutrality equation. The deviation of the fit from the measurement data at low temperatures is due to instability in the high resistance measurements in the Hall-effect measurement system. At low temperatures,

the free electrons are bound to the donors and the sample conductivity decreases. The Hall-effect measurement also provides temperature dependence of the carrier mobility (not shown) which shows that carrier mobility decreases with decreasing temperature below approximately 200 K. This decreasing trend has been reported in other experiments and it indicates strong contribution of ionized impurity scattering in the carrier-transport dynamics [9,47,49].

The fitting of free-carrier density of the Al-N sample using Eq. 8 results in the doping concentration of, $N_D = 1.31 \times 10^{19} \text{ cm}^{-3}$ and $N_{\text{comp},A} = 3.37 \times 10^{18} \text{ cm}^{-3}$ for the epilayer of the Al-N sample. While the dopant concentration is in good agreement with the TOF SIMS measurement, the density of compensating centers is higher than the acceptor concentration. This indicates that in addition to the Al acceptors, intrinsic defects are contributing to the compensation, boosting the density of ionized impurities and subsequently smearing the band structure. This supports the shift in emission band with increasing excitation power in the Al-N codoped sample.

The fitting results of the Hall-effect measurements also provide the ionization energies of the N dopant states where $\Delta E_{D,h} = 32$ and $\Delta E_{D,c} = 87$ meV, which are smaller than the typical values in low doped 6H-SiC. Similarly, for the n -type substrate, on which the Al-N epilayer is grown, $N_D = 3.97 \times 10^{18} \text{ cm}^{-3}$ and $N_{\text{comp},A} = 9.6 \times 10^{17} \text{ cm}^{-3}$, which is in reasonable agreement with the TOF SIMS measurement results, where the N concentration is $5.37 \times 10^{18} \text{ cm}^{-3}$ and the B concentration is $9.5 \times 10^{17} \text{ cm}^{-3}$. The corresponding ionization energies at the hexagonal and cubic states are 47.2 and 104.2 meV, respectively. These estimates of the ionization energy agree with the reduction of the ionization energies of dopants (ΔE_{dop}) for highly doped semiconductors. ΔE_{dop} reduces with the dopant density (N_{dop}) according to $\Delta E_{\text{dop}} = \Delta E_{\text{dop},0} - \delta N_{\text{dop}}^{1/3}$ where $\Delta E_{\text{dop},0}$ is the dopant ionization energy at low doping levels and δ is a constant. The estimated value of δ is 2.3×10^{-8} and $2.4 \times 10^{-8} \text{ eV cm}$ for the epilayer and substrate of the Al-N codoped 6H-SiC sample, respectively. These values are similar to those reported by Kimoto *et al.* [1] and Bustarret *et al* [50].

D. Temperature dependence of the PL spectra

Finally, we observe that the PL spectra red shifts with increasing temperature at a given incident power. Figure 7(a) shows the normalized PL spectra of an Al-N codoped sample at different temperatures. It can be clearly observed that the PL peak shifts toward lower energy as we increase the temperature. We note that spectral shift can also be caused by changes in the emission mechanisms. To exclude the impact of the change of the ratio of the different mechanisms, the emission spectra of each emission component is analyzed by resolving the

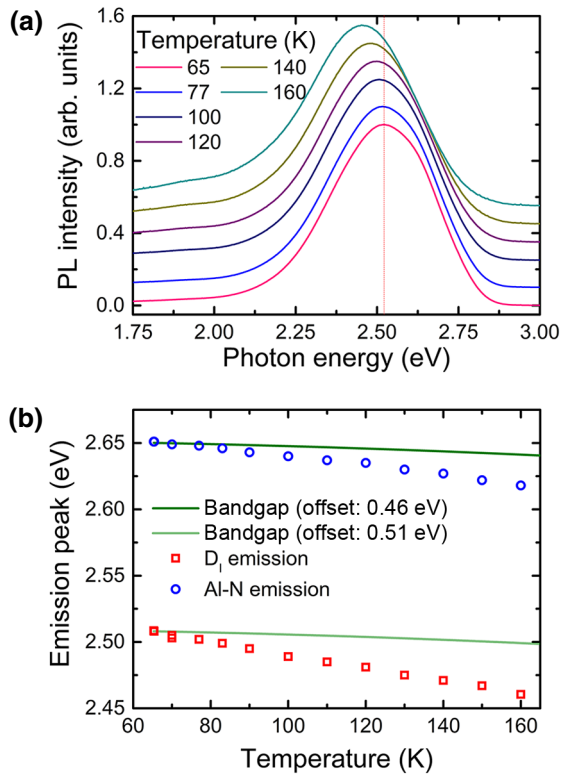


FIG. 7. (a) Photoluminescence spectra of the Al-N doped sample at various temperatures. The PL spectra are shifted vertically for clarity. (b) Emission peak energy of the Al-N DAP emission and D_1 emission as a function of temperature. The green and the light green curves indicate the bandgap of 6H-SiC as a function of temperature offset vertically by 0.46 and 0.51 eV, respectively. The curves are plotted following the reported empirical formula for the bandgap narrowing [1].

measured spectrum into its components. All the emission components are shifted to lower energies with increasing temperature. In the temperature range of Fig. 7, the prominent emission mechanisms are DAP and D_1 center emissions. The observed shifts of the PL emission peaks as a function of temperature are shown in Fig. 7(b). The PL peak shifts by approximately 5 nm for DAP emission and by 10 nm for the D_1 emission as the temperature increases from 65 to 160 K.

Bandgap narrowing with increasing temperature would also result in red shift of the PL emission and the extent of the shift is expected to follow the bandgap narrowing, which is given by the empirical expression, $E_g(T) = E_{g0} - \frac{aT^2}{(T+b)}$, where T is the temperature, $E_{g0} = 3.02$ eV, $a = 8.2 \times 10^{-4}$ eV K $^{-1}$, and $b = 1.8 \times 10^3$ K [1]. The bandgap energy as a function of temperature with vertical offsets to match the measured emission peaks of the Al-N DAP and D_1 emissions are shown with the green and light green curves, respectively. The change in bandgap between 77 and 160 K is only 8 meV while the measured shift in Al-N DAP emission is 30 meV. It can

be clearly seen that the bandgap narrowing alone cannot account for the measured peak shifts.

The peak shift toward lower energy with increasing temperature can be explained by the fluctuation potential model. The capture cross sections of free carriers at the recombination centers are not uniform due to the randomly distributed potential wells of various depths. The capture probability of the free carriers by the impurities is smaller in the deeper potential at low temperatures [27]. In the presence of the fluctuating potential, the distribution of carriers cannot be defined by a single Fermi level but a quasi-Fermi-level of states. With increasing temperature, the situation relaxes with eventual establishment of a single Fermi level. Therefore, photon energy obtained with a constant excitation power shifts to the lower energies with an increase of the temperature because of a higher involvement of the deeper potential wells.

Both the temperature and excitation power-dependent PL-spectra analysis demonstrate the formation of potential fluctuations due to the high density of ionized impurities in SiC. Low energy states near the conduction band are formed at regions of low potential and the high states near the valence band are formed at regions of high potential, which means that they are spatially separated [51]. Consequently, the DAP recombination in the distorted band states will involve the tunneling process. The tunneling process slows the radiative recombination process and thus affects the emission efficiency [34].

The potential fluctuation affects both photon emission and absorption properties and thus alters the optical spectroscopy of highly doped and compensated semiconductors, such as intrinsic and extrinsic defect analysis. Furthermore, in the presence of potential fluctuations, charge transport changes from band conduction to hopping transport, which influences electronic and photonic device performances. The depletion regions in the p - n and Schottky junctions have typically high density of ionized impurities. Thus, potential fluctuations play a big role in optoelectronic device characteristics. The demonstrated emission wavelength shifts can be used to develop tunable photon sources in SiC. For example, by controlling the free-carrier density in an optical excitation, potential fluctuation can be used to achieve wavelength tunable single phonon emission in integrated quantum photonic circuits [52].

IV. CONCLUSION

Detailed investigation of the excitation power and temperature dependences of the PL emission in Al-N codoped and B-N codoped 6H-SiC samples are performed. A simplified rate-equation model where several electron-hole recombination mechanisms are considered explains a sublinear power-law dependence of PL intensity on the excitation power. We show that the exponent in the power-law fitting carries essential information about

carrier relaxation mechanisms. A very low power exponent ($k = 0.3$) in a B-N codoped sample at RT indicates that Auger recombination involving nonequilibrium free carriers is the dominant nonradiative carrier-dissipation mechanism. In the Al-N codoped sample ($0.6 < k < 1$), the contribution of Auger recombination manifests as weaker than that of the B-N codoped sample. This is attributed to the high density of ionized impurities, which leads to a rapid capture of the free carriers to the acceptor and donor states in competition with the Auger recombination and strong contributions from nonradiative traps.

In addition, the excitation power-dependent analysis of emission spectra of the Al-N codoped sample shows a band shift to higher energy with increasing excitation intensity and a shift to lower energy with increasing temperature. The peak emission wavelength decreases by up to 10 nm as the sample temperature increases from 65 to 160 K. A significant peak shift of approximately 16 meV per decade increase in excitation power is measured. We explained the band shifts by the electrostatic potential fluctuation due to the high density of ionized impurity. Hall-effect measurements confirm the high density of ionized impurities. The Hall-effect measurement also reveals that dopant ionization energy decreases by approximately 53 meV due to the high dopant density. The potential fluctuation influences not only the photoemission property but also the nonequilibrium charge transport. Thus, it has broad implications for SiC-based electronic and photonic devices and needs to be considered in future device designs.

The investigations could lead to realization of wavelength tunable SiC-based light sources for many potential applications where the excellent material property of SiC is essential, such as high-power LEDs, all-SiC-based integrated circuits, biocompatible *in vivo* illumination, and single photon sources for quantum technologies.

ACKNOWLEDGMENTS

The work is supported by the Independent Research Fund Denmark (No. 8022-00294B). The authors acknowledge Associate Professor Syväjärvi and Dr. Jokubavicius from IFM, Linköping University for growing the 6H-SiC epilayers. We thank Dr. Schuh and Professor Wellmann from Friedrich-Alexander University Erlangen-Nürnberg (FAU) for providing source material for the epilayer growth. The authors would also like to thank Dr. Norman of King Fahd University of Petroleum and Minerals for the TOF SIMS measurements. The authors declare no competing financial interest.

-
- [1] T. Kimoto and J. A. Cooper, *Fundamentals of Silicon Carbide Technology* (John Wiley & Sons, Inc., Singapore, 2014).
- [2] W. Lu, Y. Ou, E. M. Fiordaliso, Y. Iwasa, V. Jokubavicius, M. Syväjärvi, S. Kamiyama, P. M. Petersen, and H.

- Ou, White light emission from fluorescent SiC with porous surface, *Sci. Rep.* **7**, 9798 (2017).
- [3] S.-Y. Zhuo, X.-C. Liu, T.-X. Xu, C.-F. Yan, and E.-W. Shi, Strong correlation between B-Al-N doping concentration fluctuation and photoluminescence effects of f-SiC, *AIP Adv.* **8**, 075130 (2018).
- [4] H. Ou, Y. Ou, A. Argyraki, S. Schimmel, M. Kaiser, P. Wellmann, M. K. Linnarsson, V. Jokubavicius, J. Sun, R. Liljedahl, and M. Syväjärvi, Advances in wide bandgap SiC for optoelectronics, *Eur. Phys. J. B* **87**, 58 (2014).
- [5] A. Lohrmann, N. Iwamoto, Z. Bodrog, S. Castelletto, T. Ohshima, T. J. Karle, A. Gali, S. Praver, J. C. McCallum, and B. C. Johnson, Single-photon emitting diode in silicon carbide, *Nat. Commun.* **6**, 1 (2015).
- [6] M. Atatüre, D. Englund, N. Vamivakas, S.-Y. Y. Lee, and J. Wrachtrup, Material platforms for spin-based photonic quantum technologies, *Nat. Rev. Mater.* **3**, 38 (2018).
- [7] A. T. Tarekegne, B. Zhou, K. Kaltenecker, K. Iwaszczuk, S. Clark, and P. U. Jepsen, Terahertz time-domain spectroscopy of zone-folded acoustic phonons in 4H and 6H silicon carbide, *Opt. Express* **27**, 3618 (2019).
- [8] Y. Zheng, M. Pu, A. Yi, B. Chang, T. You, K. Huang, A. N. Kamel, M. R. Henriksen, A. A. Jørgensen, X. Ou, and H. Ou, High-quality factor, high-confinement microring resonators in 4H-silicon carbide-on-insulator, *Opt. Express* **27**, 13053 (2019).
- [9] A. T. Tarekegne, K. J. Kaltenecker, P. Klarskov, K. Iwaszczuk, W. Lu, H. Ou, K. Norrman, and P. U. Jepsen, Subcycle nonlinear response of doped 4 H silicon carbide revealed by Two-dimensional terahertz spectroscopy, *ACS Photonics* **7**, 221 (2020).
- [10] Y. Zheng, M. Pu, A. Yi, X. Ou, and H. Ou, 4H-SiC microring resonators for nonlinear integrated photonics, *Opt. Lett.* **44**, 5784 (2019).
- [11] J. R. Weber, W. F. Koehl, J. B. Varley, A. Janotti, B. B. Buckley, C. G. Van de Walle, and D. D. Awschalom, Defects in SiC for quantum computing, *J. Appl. Phys.* **109**, 102417 (2011).
- [12] C. P. Anderson, A. Bourassa, K. C. Miao, G. Wolfowicz, P. J. Mintun, A. L. Crook, H. Abe, J. U. Hassan, N. T. Son, T. Ohshima, and D. D. Awschalom, Electrical and optical control of single spins integrated in scalable semiconductor devices, *Science* **366**, 1225 (2019).
- [13] D. M. Lukin, C. Dory, M. A. Guidry, K. Y. Yang, S. D. Mishra, R. Trivedi, M. Radulaski, S. Sun, D. Vercruysee, G. H. Ahn, and J. Vučković, 4H-silicon-carbide-on-insulator for integrated quantum and nonlinear photonics, *Nat. Photonics* **1**, 1 (2019).
- [14] V. N. Kurlov, *Ref. Modul. Mater. Sci. Mater. Eng.* (Elsevier, Amsterdam, 2016), pp. 1–11.
- [15] I. Bhat, *Wide Bandgap Semicond. Power Devices* (Elsevier, Amsterdam, 2019), pp. 43–77.
- [16] S. A. Kukushkin, A. V. Osipov, V. N. Bessolov, B. K. Medvedev, V. K. Nevolin, and K. A. Tcarik, Substrates for epitaxy of gallium nitride: New materials and techniques, *Rev. Adv. Mater. Sci.* **17**, 1 (2008).
- [17] S. Kamiyama, T. Maeda, Y. Nakamura, M. Iwaya, H. Amano, I. Akasaki, H. Kinoshita, T. Furusho, M. Yoshimoto, T. Kimoto, J. Suda, A. Henry, I. G. Ivanov, J. P. Bergman, B. Monemar, T. Onuma, and S. F. Chichibu, Extremely high quantum efficiency of donor-acceptor-pair

- emission in N-and-B-doped 6H-SiC, *J. Appl. Phys.* **99**, 093108 (2006).
- [18] Y. Wei and H. Ou, Photoluminescence quantum yield of fluorescent silicon carbide determined by an integrating sphere setup, *ACS Omega* **4**, 15488 (2019).
- [19] S. Li, L. Wang, N. Hirotsuki, and R. Xie, Color conversion materials for high-brightness laser-driven solid-state lighting, *Laser Photon. Rev.* **12**, 1800173 (2018).
- [20] S. P. Denbaars, D. Feezell, K. Kelchner, S. Pimputkar, C. C. Pan, C. C. Yen, S. Tanaka, Y. Zhao, N. Pfaff, R. Farrell, M. Iza, S. Keller, U. Mishra, J. S. Speck, and S. Nakamura, Development of gallium-nitride-based light-emitting diodes (LEDs) and laser diodes for energy-efficient lighting and displays, *Acta Mater.* **61**, 945 (2013).
- [21] H. He, Q. Yu, H. Li, J. Li, J. Si, Y. Jin, N. Wang, J. Wang, J. He, X. Wang, Y. Zhang, and Z. Ye, Exciton localization in solution-processed organolead trihalide perovskites, *Nat. Commun.* **7**, 10896 (2016).
- [22] N. M. Gasanly, A. Serpengüzel, A. Aydinli, O. Gürlü, and I. Yilmaz, Donor-acceptor pair recombination in AgIn₅S₈ single crystals, *J. Appl. Phys.* **85**, 3198 (1999).
- [23] D. E. Cooper, J. Bajaj, and P. R. Newman, Photoluminescence spectroscopy of excitons for evaluation of high-quality CdTe crystals, *J. Cryst. Growth* **86**, 544 (1988).
- [24] W. S. Shi, B. Cheng, L. Zhang, and E. T. Samulski, Influence of excitation density on photoluminescence of zinc oxide with different morphologies and dimensions, *J. Appl. Phys.* **98**, 083502 (2005).
- [25] H. Wang, Z. Ji, S. Qu, G. Wang, Y. Jiang, B. Liu, X. Xu, and H. Mino, Influence of excitation power and temperature on photoluminescence in InGaN/GaN multiple quantum wells, *Opt. Express* **20**, 3932 (2012).
- [26] T. Schmidt, K. Lischka, and W. Zulehner, Excitation-power dependence of the near-band-edge photoluminescence of semiconductors, *Phys. Rev. B* **45**, 8989 (1992).
- [27] P. W. Yu, Excitation-dependent emission in Mg-, Be-, Cd-, and Zn-implanted GaAs, *J. Appl. Phys.* **48**, 5043 (1977).
- [28] H. P. Gislason, B. H. Yang, and M. Linnarsson, Shifting photoluminescence bands in high-resistivity Li-compensated GaAs, *Phys. Rev. B* **47**, 9418 (1993).
- [29] B. Guo, Z. R. Qiu, and K. S. Wong, Intensity dependence and transient dynamics of donor-acceptor pair recombination in ZnO thin films grown on (001) silicon, *Appl. Phys. Lett.* **82**, 2290 (2003).
- [30] P. Bäume, J. Gutowski, D. Wiesmann, R. Heitz, A. Hoffmann, E. Kurtz, D. Hommel, and G. Landwehr, Intensity-dependent energy and line shape variation of donor-acceptor-pair bands in ZnSe:N at different compensation levels, *Appl. Phys. Lett.* **67**, 1914 (1995).
- [31] B. I. Shklovskii and A. L. Efros, *Electronic Properties of Doped Semiconductors* (Springer Berlin Heidelberg, Berlin, Heidelberg, 1984).
- [32] Y. Ou, V. Jokubavicius, M. Linnarsson, R. Yakimova, M. Syväjärvi, and H. Ou, Characterization of donor-acceptor-pair emission in fluorescent 6H-SiC, *Phys. Scr.* **T148**, 014003 (2012).
- [33] E. F. Schubert, I. D. Goepfert, W. Grieshaber, and J. M. Redwing, Optical properties of Si-doped GaN, *Appl. Phys. Lett.* **71**, 921 (1997).
- [34] I.-H. Lee, J. J. Lee, P. Kung, F. J. Sanchez, and M. Razeghi, Band-gap narrowing and potential fluctuation in Si-doped GaN, *Appl. Phys. Lett.* **74**, 102 (1999).
- [35] T. Makino, Y. Segawa, S. Yoshida, A. Tsukazaki, A. Ohtomo, and M. Kawasaki, Gallium concentration dependence of room-temperature near-band-edge luminescence in n-type ZnO:Ga, *Appl. Phys. Lett.* **85**, 759 (2004).
- [36] M. Syväjärvi and R. Yakimova, *Compr. Semicond. Sci. Technol.* (Elsevier, Amsterdam, 2011), pp. 202–231.
- [37] M. Ikeda, T. Hayakawa, S. Yamagiwa, H. Matsunami, and T. Tanaka, Fabrication of 6H-SiC light-emitting diodes by a rotation dipping technique: Electroluminescence mechanisms, *J. Appl. Phys.* **50**, 8215 (1979).
- [38] M. V. B. Pinheiro, E. Rauls, U. Gerstmann, S. Greulich-Weber, H. Overhof, and J. M. Spaeth, Silicon vacancy annealing and DI luminescence in 6H-SiC, *Phys. Rev. B* **70**, 245204 (2004).
- [39] A. T. Tarekne, K. Norrman, V. Jokubavicius, M. Syväjärvi, P. Schuh, P. Wellmann, and H. Ou, Impacts of carrier capture processes in the thermal quenching of photoluminescence in Al-N co-doped SiC, *Appl. Phys. B* **125**, 172 (2019).
- [40] Y. Wei, A. T. Tarekne, and H. Ou, Double D-centers related donor-acceptor-pairs emission in fluorescent silicon carbide, *Opt. Mater. Express* **9**, 295 (2019).
- [41] G. Pensl and W. J. Choyke, Electrical and optical characterization of SiC, *Phys. B Condens. Matter* **185**, 264 (1993).
- [42] M. Ikeda, H. Matsunami, and T. Tanaka, Site effect on the impurity levels in 4H, 6H, and 15R SiC, *Phys. Rev. B* **22**, 2842 (1980).
- [43] W. J. Choyke and L. Patrick, Exciton recombination radiation and phonon spectrum of 6H SiC, *Phys. Rev.* **127**, 1868 (1962).
- [44] W. Suttrop, G. Pensl, and P. Lanig, Boron-related deep centers in 6H-SiC, *Appl. Phys. A Solids Surfaces* **51**, 231 (1990).
- [45] A. A. Lebedev, Deep level centers in silicon carbide: A review, *Semiconductors* **33**, 107 (1999).
- [46] Y. Wei, A. T. Tarekne, and H. Ou, Influence of negative-U centers related carrier dynamics on donor-acceptor-pair emission in fluorescent SiC, *J. Appl. Phys.* **124**, 054901 (2018).
- [47] J. Pernot, W. Zawadzki, S. Contreras, J. L. Robert, E. Neyret, and L. Di Cioccio, Electrical transport in n-type 4H silicon carbide, *J. Appl. Phys.* **90**, 1869 (2001).
- [48] W. Suttrop, G. Pensl, W. J. Choyke, R. Stein, and S. Leibenzeder, Hall effect and infrared absorption measurements on nitrogen donors in 6H-silicon carbide, *J. Appl. Phys.* **72**, 3708 (1992).
- [49] W. Götz, A. Schöner, G. Pensl, W. Suttrop, W. J. Choyke, R. Stein, and S. Leibenzeder, Nitrogen donors in 4H-silicon carbide, *J. Appl. Phys.* **73**, 3332 (1993).
- [50] P. Achatz, J. Pernot, C. Marcenat, J. Kacmarcik, G. Ferro, and E. Bustarret, Doping-induced metal-insulator transition in aluminum-doped 4H silicon carbide, *Appl. Phys. Lett.* **92**, 072103 (2008).
- [51] D. Redfield, J. P. Wittke, and J. I. Pankove, Luminescent properties of energy-band-tail states in GaAs:Si, *Phys. Rev. B* **2**, 1830 (1970).
- [52] A. W. Elshaari, I. E. Zadeh, A. Fognini, M. E. Reimer, D. Dalacu, P. J. Poole, V. Zwiller, and K. D. Jöns, On-chip single photon filtering and multiplexing in hybrid quantum photonic circuits, *Nat. Commun.* **8**, 379 (2017).